

Cite this: DOI: 00.0000/xxxxxxxxxx

Large Amplitude Charge Noise and Random Telegraph Fluctuations in Room-Temperature Graphene Single-Electron Transistors

Jasper P. Fried,^a Xinya Bian,^a Jacob L. Swett,^a Ivan I. Kravchenko,^b G. Andrew D. Briggs,^a and Jan A. Mol^{a, c}

Received Date

Accepted Date

DOI: 00.0000/xxxxxxxxxx

We analyze the noise in liquid-gated, room temperature, graphene quantum dots. These devices display extremely large noise amplitudes. The observed noise is explained in term of a charge noise model by considering fluctuations in the applied source-drain and gate potentials. We show that the liquid environment and substrate have little effect on the observed noise and as such attribute the noise to charge trapping/detrapping at the disordered graphene edges. The trapping/detrapping of individual charges can be tuned by gating the device, which can result in stable two-level fluctuations in the measured current. These results have important implications for the use of electronic graphene nanodevices in e.g. single-molecule biosensing.

1 Introduction

Graphene nanostructures have received significant attention in recent years for use as single-molecule biosensors^{1,2}. Interest in these devices has often focused on DNA sequencing applications^{3–5}, however, these devices are also being extended for an array of studies on the dynamics and interactions of biomolecules^{6–10}. Such devices generally rely on detecting changes in the current through a graphene nanostructure due to a nearby analyte of interest. Clearly an important consideration in the further development of these devices is their noise characteristics. Noise in microscale graphene structures has been well studied over the past decade¹¹. These works have demonstrated the importance of the device substrate, surface contamination, and graphene defects in determining the noise characteristics^{12–15}. To date, there have been relatively few studies on the noise characteristics of graphene structures with sizes on the order of a few nanometers. Moreover, any such studies have typically been performed at cryogenic temperatures and under high vacuum^{16,17}.

Here we analyze the noise characteristics of a graphene quantum dot (considered as an example graphene nanostructure) at room temperature in liquid environments. The noise observed in these devices is several orders of magnitude larger than that seen in micron sized graphene ribbons. The observed noise can be explained in terms of a charge noise model, however, in contrast

to previous studies^{16,18} we demonstrate the need to incorporate fluctuations in the source-drain voltage. We show that the noise is largely independent of the liquid environment and the substrate. As such we attribute the noise to charge trapping/detrapping at the disordered graphene edges. Changing the gate potential influences the trapping/detrapping of individual charges, which in some cases can lead to two-level fluctuations in the current level. These noise characteristics will need to be carefully considered if graphene nanodevices are to reach their full potential in applications such as single-molecule biosensing^{2,4}.

2 Experimental

A schematic of our device geometry is shown in Fig. 1(a) with the basic measurement setup depicted in Fig. 1(b). We start with a graphene nano-constriction on a SiN_x/SiO₂/Si substrate. The graphene nano-constriction is patterned via electron beam lithography and subsequent oxygen plasma etching. A PMMA passivation layer (with windows over the graphene and contact pads) is used to cover the gold electrodes to reduce Faradaic currents¹⁹ and capacitive noise [see Supporting Information 1 (SI1)]. Graphene quantum dots are then created from the graphene nano-constriction via a feedback-controlled electroburning technique described elsewhere^{20,21}. This technique relies on the oxidation/sublimation of graphene due to Joule heating when passing large current densities through the graphene²². While feedback-controlled electroburning is commonly used to create graphene nanogaps, the probabilistic nature of the oxidation/sublimation process means that graphene quantum dots (GQD) can also be created²³. The nanoscale structure of electroburnt graphene quantum dots is largely unknown due to

^a Department of Materials, University of Oxford, Oxford, OX1 3PH, United Kingdom

^b Center for Nanophase Materials Science, Oak Ridge National Laboratory, Oak Ridge, TN 37830, United States of America

^c Department of Physics, Queen Mary University London, London, E1 4NS, United Kingdom

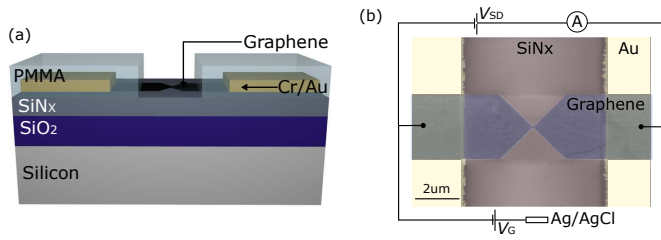


Fig. 1 (a) A schematic depicting our device geometry. (b) A schematic of our measurement setup along with a false color Scanning Electron Micrograph of a fabricated graphene nano-constriction prior to electroburning (PMMA passivation layer not in image).

their small lateral dimensions ($\sim 2\text{nm}$)^{23,24} (i.e. can not be easily imaged via AFM or SEM), however, these devices presumably consists of a graphene island connected by nanoscale graphene electrodes. GQD devices are determined by measuring the current as a function of gate voltage applied via the silicon substrate and looking for features of sequential electron transport through a quantum dot^{23,25}. Appropriate devices are then wirebonded to a printed circuit board and loaded into a custom made fluidic cell with an upstream Ag/AgCl electrode to control the gate potential. After filling the flow cell with a 1M KCl solution, the source-drain (V_{SD}) and gate (V_G) voltages are swept while measuring 2s long current-time ($I-t$) traces at each applied voltage using a low-noise current amplifier (Axopatch 200B).

3 Results and Discussion

Figure 2(a) plots the mean current as a function of V_{SD} and V_G . Such a plot is commonly referred to as a stability diagram. The stability diagram shown here demonstrates behavior typical of single-electron transport through a quantum dot²⁵. Namely, we observe a high-current region indicative of resonant electron transport whereby an energy level of the quantum dot is aligned within the energy levels of the electrodes. Outside of this region, we observe a low-current region indicative of Coulomb blockade whereby the electrostatic energy required to add an electron to the quantum dot precludes electron transport. From the stability diagram we can obtain a lower bound for the addition energy of this quantum dot of 200meV. This is well above the thermal energy, $k_B T$, at 300K (approximately 26meV), enabling the observation of Coulomb blockade at room temperature. The high addition energy results from the nanoscale nature of these GQDs with a previous report estimating their size to be on the order of 2nm²⁴. As shown in SI1, despite using a PMMA pasivation layer to cover the gold electrodes, we observe a small Faradaic current at large negative voltages. As such, the remainder of the discussion in this work will concentrate on gate voltages in the region $-0.3\text{V} \leq V_G \leq 0.1\text{V}$. The ability to control the electron transport through a graphene quantum dot via electrolyte gating has been reproduced across several devices (SI2).

Figure 2(b) and (c) show slices through the stability diagram for a given V_{SD} and V_G respectively. Fits to the measured data based on a rate equation model²⁶ are also shown in these plots (as discussed above there is a deviation from the fit for $V_G < -0.3\text{V}$ due to the presence of Faradiac current here). As described in

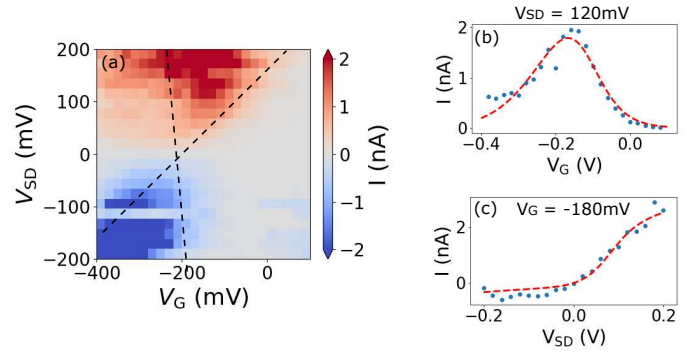


Fig. 2 (a) Stability diagram of the measured current as a function of the source-drain voltage and the gate voltage. The dashed lines represent the edges of the resonant transport regime extracted from the Marcus fits. (b) Current as a function of gate voltage for $V_{SD}=120\text{mV}$. (c) Current as a function of source-drain voltage for $V_G=-180\text{mV}$. The red curves in (b) and (c) show the fits to the rate equation.

SI3, the rate constants are determined from semi-classical Marcus theory which accounts for the structural reorganization energy of the graphene quantum dot and its solvation shell upon charge transfer²⁷. These fits will be used below to analyze the noise characteristics of our devices. The fits also provide estimates for the ratio of the capacitive coupling to the source (C_S), drain (C_D) and gate (C_G) electrodes²⁵. We obtain $C_S/C_G = 0.36$ and $C_D/C_G = 0.16$. Different values of C_S and C_D result from asymmetries between the source and drain graphene electrodes contacting the GQD resulting from the probabilistic nature of the electroburning process. Due to the high ionic concentration solution used in this work (1M KCl) the electrochemical double layer which forms at the graphene-ionic solution interface is very short (Debye length $\lambda = 0.304\text{nm}$)²⁸. This leads to a large gate capacitance in our devices (i.e. $C_G > C_{S/D}$ as confirmed above from our fits) which results in the energy levels of the quantum dot being closely coupled to the gate potential.

Figure 3(a) shows an example $I-t$ trace taken during these measurements. The corresponding normalized noise spectrum of the $I-t$ trace is shown in Fig. 3(b). We observe a $1/f$ noise spectrum that is ubiquitous in nanoscale electronic systems. Although the source of such noise varies depending on the system being mea-

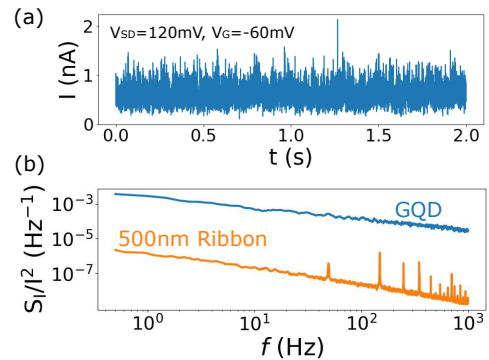


Fig. 3 (a) An example current-time trace at $V_{SD}=120\text{mV}$, $V_G=-60\text{mV}$. (b) Noise spectrum from the graphene quantum dot and a 500nm wide, $10\mu\text{m}$ long graphene ribbon.

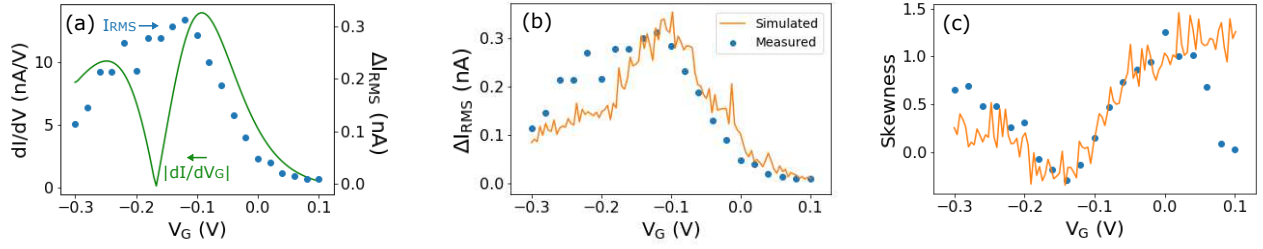


Fig. 4 (a) RMS current noise as a function of gate voltage for $V_{\text{SD}}=120$ mV (blue dots, right axis), plotted against the transconductance (green line, left axis). (b) Measured and simulated RMS current noise as a function of V_G for $V_{\text{SD}}=120$ mV. (c) Measured and simulated skewness of the I - t traces as a function of V_G for $V_{\text{SD}}=120$ mV.

sured, it is generally accepted that $1/f$ noise in these systems results from the superposition of two-level fluctuators with different time constants^{29,30}. Figure 3(b) also shows the normalized noise spectrum from a 500 nm wide, 10 μm long, graphene ribbon (fabricated via electron beam lithography using the same process as our graphene nanoconstriction). The measured noise is 3-4 orders of magnitude larger in the graphene quantum dot than the 500 nm wide graphene ribbon. The noise in 30 nm wide graphene nanoribbons has also been reported to be 2-3 orders of magnitude lower than what we measure for a GQD³¹, highlighting the dramatic increase in noise when shrinking the graphene dimensions down to a few nanometers. This increased noise magnitude partially results from the greater sensitivity of a GQD to changes in the electric potential compared to micron-scale graphene ribbons (see SI4). Moreover, as will be demonstrated below it is likely that different mechanisms dominate the noise in these two device geometries. Namely, for a GQD the noise is predominately due to charge trapping at the disordered graphene edges. However, for micron-scale graphene ribbons where the graphene edges are far from the conduction channel charge noise originating from the substrate and surface contamination dominate the measured noise¹¹.

Previous studies on quantum dots^{16,18} (as well as graphene ribbons¹³ and carbon nanotubes³²) have reported that ΔI_{RMS} scales with the magnitude of the transconductance ($|dI/dV_G|$). This implies that the noise results from nearby charge fluctuations that act to gate the device. In Fig. 4(a) we plot the measured rms noise along with $|dI/dV_G|$ as calculated from the fits to the rate equation described above. In our case ΔI_{RMS} clearly does not scale with the transconductance, especially at the center of the resonant transport regime. We postulate that this is because fluctuations in the V_{SD} must be considered in addition to fluctuations in V_G . Indeed, below we will show that by considering fluctuations in both V_{SD} and V_G we can reproduce the measured noise behavior. Given that the gate potential is closely coupled to the energy level of the quantum dot, one can consider fluctuations in V_G as corresponding to changes in the energy level of the quantum dot. Similarly, fluctuations in V_{SD} correspond to changes in the local Fermi level of the nanoscale graphene electrodes connecting the quantum dot.

To show that the observed noise can be accurately described by fluctuations in V_G and V_{SD} we have simulated I - t traces. Namely,

using the fits to the rate equation described above we can calculate the current at any source-drain and gate voltage as $I(V_{\text{SD}}, V_G)$. For given fluctuations ΔV_{SD} and ΔV_G the resulting current can also be calculated as $I(V_{\text{SD}} + \Delta V_{\text{SD}}, V_G + \Delta V_G)$. We assume that ΔV_{SD} and ΔV_G have a $1/f$ spectrum and a Gaussian distribution. We calculate the current for 5000 consecutive fluctuations to create a simulated I - t trace. As shown in Fig. 4(b), we find that potential fluctuations in both V_{SD} and V_G with a standard deviation of 13 mV reproduces the measured rms-noise across the range of applied gate voltages fairly well.

In our devices the current depends non-linearly on both V_{SD} and V_G . One result of this is that symmetric fluctuations in V_{SD} and V_G lead to an asymmetry in the I - t traces. This asymmetry can be seen in the I - t trace shown in Fig. 3(a) where the distribution is skewed towards larger current values. To quantify this asymmetry we calculate the skewness of the I - t traces. The skewness (g_1) is calculated as $g_1 = m_3/m_2^{3/2}$ where m_r is the r^{th} moment about the mean and can be calculated for a distribution of N points with values x_i by $m_r = 1/N \sum (x_i - \bar{x})^r$ ³³. A skewness of zero indicates a symmetric distribution, while a skewness greater (smaller) than zero indicates there is more weight towards higher (lower) current values.

In Fig. 4(c) we plot the skewness of the measured I - t traces as a function of gate voltage for $V_{\text{SD}}=120$ mV. Away from the resonant transport regime the skewness is positive indicating that the current changes faster when increasing the current compared to decreasing the current. Moving towards the resonant transport regime the skewness becomes zero and even reaches a negative value at the center of the resonant transport regime. As shown in Fig. 4(c), the simulated I - t traces for the fluctuations in V_{SD} and V_G described above closely reproduce the behavior in the measured skewness across the range of applied V_G (except at large values of V_G where the current approaches zero and the noise of the measurement system starts to dominate). The need to incorporate fluctuations in V_{SD} to explain the measured noise is again highlighted by considering the skewness in the I - t traces. In particular, when operating at the center of the resonant transport regime fluctuations in V_G would result only in negative changes in the current. This would lead to a very large negative value of the skewness. In reality, we observe a skewness close to zero (slightly negative) at the center of the resonant transport regime since fluctuations in V_{SD} also contribute strongly to the noise here. Such

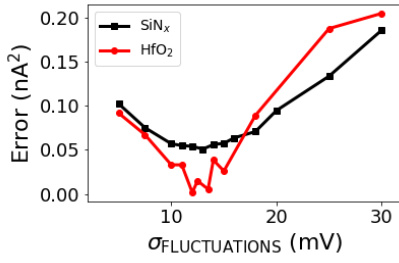


Fig. 5 Comparison of the sum of the squared residuals between the simulated and measured rms noise (labelled error) as a function of the standard deviation of the simulated potential fluctuations for a device on HfO₂ and Si_x.

analysis of the skewness of the I - t traces hasn't been considered before in previous studies on similar systems^{13,16,18}. As shown here analyzing the skewness of the I - t traces is another useful tool in isolating contributions to the observed noise, especially in non-linear systems such as the GQD considered here.

To determine the source of charge fluctuations in our devices we have measured GQDs on a different substrate. In these devices the GQD was supported by 10nm of HfO₂, below which was a 30nm thick Au electrode. The Au electrode was used to gate the GQD and the device was measured in Air. If the charge noise in our devices originated from the substrate one would expect the noise in this device to be different for several reasons. Firstly, HfO₂ has a significantly different dielectric constant to SiN_x resulting in different charge screening, secondly, HfO₂ would be expected to have a different density of charge traps than SiN_x, and thirdly, the Au electrode will act to screen potential fluctuations from charge traps farther than 10nm from the GQD. However, as shown in SI6, we find that we can replicate the measured noise behavior in these devices by applying similar potential fluctuations to those described for the SiN_x devices (after accounting for the different gate capacitances of the devices). Indeed, in Fig. 5 we plot the sum of the squared residuals between the measured and simulated rms noise as a function of the standard deviation of the applied potential fluctuations for the HfO₂ device and the SiN_x device. The minimum of this plot corresponds to the potential fluctuations that give the least squares fit between the measured and the simulated data. Clearly, the difference between simulated and measured data are minimized by similar potential fluctuations for both device geometries suggesting that the substrate and electrolyte environment has little effect on the measured noise. These results are in agreement with a previous study on the noise graphene quantum dots at cryogenic temperatures where it was demonstrated that suspending the device didn't affect the noise level¹⁶. Here, it was postulated that the noise results from charge trapping/detrapping at the disordered graphene edges. Based on the results described above we believe charge trapping at disordered graphene edges are also the dominant source of noise in our devices. However, charge noise originating from the graphene surface or at the graphene-substrate interface can not be discounted from our measurements.

An important observation in our devices is that at specific volt-

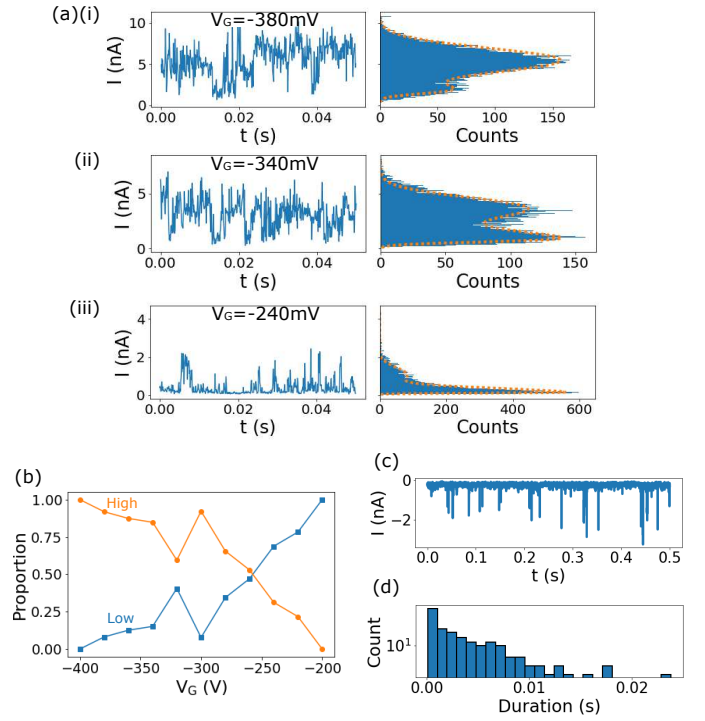


Fig. 6 (a) Examples of two level fluctuations in I - t traces and their corresponding current value histograms for $V_{SD}=200$ mV and (i) $V_G=-380$ mV, (ii) $V_G=-340$ mV, and (iii) $V_G=-240$ mV. The dashed orange lines show fits to the histogram using a double skewed Gaussian distribution. (b) Change in occupation of the up and down-current states as a function of gate voltage. (c) Examples of sharp current spikes in these devices and (d) the distribution of the duration of these current spikes.

ages we observe two-level fluctuations (TLFs) in the current level. Such TLFs are yet to be reported on graphene nanodevices at room temperature¹⁷. Since charge fluctuators are generally thermally activated^{2,34}, operating at room temperature usually results in the sampling of a large number of fluctuators. However, since our devices have dimensions on the order of a few nanometers we sample a small number of fluctuators even at room temperature. Figure 6(a)(i)-(iii) shows examples of I - t traces demonstrating two-level fluctuations (the presence of which are more easily observed in the corresponding histograms). By changing the gate voltage we are able to tune the proportion of time spent in the high and low current states. For $V_G=-380$ mV, [Fig. 6(a)(i)] the current is predominately in the high state, for $V_G=-340$ mV [Fig. 6(a)(ii)] the current is almost evenly split between the high and low states and for $V_G=-240$ mV [Fig.6(a)(iii)] the current is predominately in the low state. We estimate the time spent in the high and low current states by fitting two skewed Gaussian distributions to the peaks in the I - t histograms [dashed orange lines in Fig. 6(a)(i)-(iii)] and integrating the area under each curve. The proportion of time spent in the high state clearly decreases with increasing V_G [Fig. 6(b)], demonstrating the ability to tune individual charge traps in our devices by the application of a gate voltage. The TLF signal observed here presumably results from the same source as the $1/f$ noise describe above. Namely, we believe it is a result of charge trapping at the disordered graphene

edges.

In some cases we observe remarkably large two-level fluctuations in the current level. This presumably results when the charge fluctuator is in very close proximity to the GQD. An example of this is shown in Fig. 6(c) where we show current spikes ~ 10 times larger than the baseline current value. As shown in Fig. 6(d), the duration of these current spikes has an exponential distribution with a time constant $\tau \sim 0.63$ ms. Many of the current spikes are limited by the bandwidth of our measurement system (10 kHz) and appear as a single point in our I - t traces. Notably, the TLF signals and current spikes shown here are very similar to signals that have been observed when using graphene nanodevices for real-time single-molecule studies^{6–8}. As such our results will need to be carefully considered in future works using graphene nanodevices for single-molecule biosensing applications.

4 Conclusion

In conclusion, we have analyzed the noise characteristics of a graphene quantum dot at room temperature in liquid environments. We explain the observed noise in terms of a charge noise model with the incorporation of fluctuations in both V_{SD} and V_G . We show that the observed noise is independent of the liquid environment and the substrate and thus likely results from the trapping/detrapping of charges at the disordered graphene edges. The fact that our devices have dimensions on the order of a few nanometers means that we sample a small number of these charge fluctuators which, in some cases, results in the observation of two-level fluctuations in the measured current. The high noise level and presence of two-level fluctuations will need to be carefully considered if graphene nanodevices are to reach their full potential in applications such as single-molecule biosensing. Although these results have been obtained for a graphene quantum dot, we believe that they are relevant to other graphene structures with dimensions on the order of a few nanometers, such as nanogaps and nanoribbons, especially if these devices possess disordered edges.

Conflicts of interest

The authors declare no conflicts of interest.

Acknowledgements

Substrate and electrode fabrication was conducted at the Center for Nanophase Materials Sciences, which is a DOE Office of Science User Facility. The authors thank Bart Limburg and Jakub Sowa for useful discussion and Kevin Lester for preparing the wafers. This work was funded by the UK EPSRC (Grant No. EP/N017188/1). JAM is a RAEng Engineering for Development Research Fellow. JPF thanks the Oxford Australia Scholarship Fund and The University of Western Australia for funding.

Notes and references

- 1 H. Arjmandi-Tash, L. A. Belyaeva and G. F. Schneider, *Chemical Society Reviews*, 2016, **45**, 476–493.
- 2 P. Puczkarski, J. L. Swett and J. A. Mol, *Journal of Materials Research*, 2017, **32**, 3002–3010.
- 3 F. Traversi, C. Raillon, S. M. Benameur, K. Liu, S. Khlybov, M. Tosun, D. Krasnozhan, A. Kis and A. Radenovic, *Nature Nanotechnology*, 2013, **8**, 939–945.
- 4 S. J. Heerema and C. Dekker, *Nature Nanotechnology*, 2016, **11**, 127–136.
- 5 J. P. Fried, J. L. Swett, X. Bian and J. A. Mol, *MRS Communications*, 2018, 1–9.
- 6 H. Wen, W. Li, J. Chen, G. He, L. Li, M. A. Olson, A. C.-H. Sue, J. F. Stoddart and X. Guo, *Science Advances*, 2016, **2**, e1601113.
- 7 C. Zhou, X. Li, Z. Gong, C. Jia, Y. Lin, C. Gu, G. He, Y. Zhong, J. Yang and X. Guo, *Nature Communications*, 2018, **9**, year.
- 8 J. Guan, C. Jia, Y. Li, Z. Liu, J. Wang, Z. Yang, C. Gu, D. Su, K. N. Houk, D. Zhang and X. Guo, *Science Advances*, 2018, **4**, eaar2177.
- 9 Y. Choi, I. S. Moody, P. C. Sims, S. R. Hunt, B. L. Corso, I. Perez, G. A. Weiss and P. G. Collins, *Science*, 2012, **335**, 319–324.
- 10 S. Sorgenfrei, C. Yang Chiu, R. L. Gonzalez, Y.-J. Yu, P. Kim, C. Nuckolls and K. L. Shepard, *Nature Nanotechnology*, 2011, **6**, 126–132.
- 11 A. A. Balandin, *Nature Nanotechnology*, 2013, **8**, 549–555.
- 12 A. A. Kaverzin, A. S. Mayorov, A. Shytov and D. W. Horsell, *Physical Review B*, 2012, **85**, year.
- 13 I. Heller, S. Chatoor, J. MaĹnnik, M. A. G. Zevenbergen, J. B. Oostinga, A. F. Morpurgo, C. Dekker and S. G. Lemay, *Nano Letters*, 2010, **10**, 1563–1567.
- 14 M. Kayyalha and Y. P. Chen, *Applied Physics Letters*, 2015, **107**, 113101.
- 15 T. Sharf, J. W. Kevek, T. DeBorde, J. L. Wardini and E. D. Minot, *Nano Letters*, 2012, **12**, 6380–6384.
- 16 X. Song, H. Li, J. You, T. Han, G. Cao, T. Tu, M. Xiao, G. Guo, H. Jiang and G. Guo, *Scientific Reports*, 2015, **5**, 8142.
- 17 P. Puczkarski, Q. Wu, H. Sadeghi, S. Hou, A. Karimi, Y. Sheng, J. H. Warner, C. J. Lambert, G. A. D. Briggs and J. A. Mol, *ACS Nano*, 2018, **12**, 9451–9460.
- 18 S. W. Jung, T. Fujisawa, Y. Hirayama and Y. H. Jeong, *Applied Physics Letters*, 2004, **85**, 768–770.
- 19 K. Healy, V. Ray, L. J. Willis, N. Peterman, J. Bartel and M. Drndić, *Electrophoresis*, 2012, **33**, 3488–3496.
- 20 F. Prins, A. Barreiro, J. W. Ruitenberġ, J. S. Seldenthuis, N. Aliaga-Alcalde, L. M. K. Vandersypen and H. S. J. van der Zant, *Nano Letters*, 2011, **11**, 4607–4611.
- 21 C. S. Lau, J. A. Mol, J. H. Warner and G. A. D. Briggs, *Phys. Chem. Chem. Phys.*, 2014, **16**, 20398–20401.
- 22 M. Abbassi, L. Pósa, P. Makk, C. Nef, K. Thodkar, A. Halbritter and M. Calame, *Nanoscale*, 2017, **9**, 17312–17317.
- 23 B. Limburg, J. O. Thomas, G. Holloway, H. Sadeghi, S. Sangtarash, I. Hou, J. Cremers, A. Narita, K. MĹijllen, C. J. Lambert, G. A. D. Briggs, J. A. Mol and H. L. Anderson, *Advanced Functional Materials*, 2018, **28**, 1803629.
- 24 A. Barreiro, H. S. J. van der Zant and L. M. K. Vandersypen, *Nano Letters*, 2012, **12**, 6096–6100.
- 25 R. Hanson, L. P. Kouwenhoven, J. R. Petta, S. Tarucha and

- L. M. K. Vandersypen, *Reviews of Modern Physics*, 2007, **79**, 1217–1265.
- 26 J. K. Sowa, J. A. Mol, G. A. D. Briggs and E. M. Gauger, *The Journal of Chemical Physics*, 2018, **149**, 154112.
- 27 J. O. Thomas, B. Limburg, J. K. Sowa, K. Willick, J. Baugh, G. A. D. Briggs, E. M. Gauger, H. L. Anderson and J. A. Mol, *arXiv:1812.07562*, 2018.
- 28 R. Netz, *The European Physical Journal E*, 2000, **3**, 131–141.
- 29 M. Kirton and M. Uren, *Advances in Physics*, 1989, **38**, 367–468.
- 30 M. B. Weissman, *Reviews of Modern Physics*, 1988, **60**, 537–571.
- 31 Y.-M. Lin and P. Avouris, *Nano Letters*, 2008, **8**, 2119–2125.
- 32 J. MÃĎnnik, I. Heller, A. M. Janssens, S. G. Lemay and C. Dekker, *Nano Letters*, 2008, **8**, 685–688.
- 33 D. Zwillinger and S. Kokoska, *CRC Standard Probability and Statistics Tables and Formulae*, Chapman and Hall, 2000.
- 34 J. Tersoff, *Nano Letters*, 2007, **7**, 194–198.